

Absence of confinement in (SrTiO₃)/(SrTi_{0.8}Nb_{0.2}O₃) superlattices

G. Bouzerar,* S. Thébaud, R. Bouzerar, S. Pailhès, and Ch. Adessi

Univ Lyon, Université Claude Bernard Lyon 1, CNRS, Institut Lumière Matière, F-69622 Lyon, France

(Received 28 September 2017; published 9 March 2018)

The reduction of dimensionality is considered an efficient pathway to boost the performances of thermoelectric materials. Quantum confinement of the carriers is expected to induce large Seebeck coefficients (S) and it also suppresses the thermal conductivity by increasing the phonon scattering processes. However, quantum confinement in superlattices is not always easy to achieve and needs to be carefully validated. In the past decade, large values of S have been measured in (SrTiO₃)/(SrTi_{0.8}Nb_{0.2}O₃) superlattices [H. Ohta *et al.*, *Nat. Mater.* **6**, 129 (2007); Y. Mune *et al.*, *Appl. Phys. Lett.* **91**, 192105 (2007)]. In the δ -doped compound, the reported S was almost six times larger than that of the bulk material. This huge increase has been attributed to the two-dimensional carrier confinement in the doped regions. Here, we demonstrate that the experimental data are well explained quantitatively assuming delocalized electrons in both in-plane and growth directions. Moreover, we rule out the confined electron hypothesis whose signature would be the suppression of the Seebeck coefficient. This strongly suggests that the presupposed confinement picture in these superlattices is unlikely.

DOI: [10.1103/PhysRevMaterials.2.035402](https://doi.org/10.1103/PhysRevMaterials.2.035402)**I. THE ISSUE OF CONFINEMENT IN SUPERLATTICES**

Over the past two decades, and because of increasing energy and environmental issues, thermoelectric materials have regained great interest owing to their ability to convert waste heat into electricity [1–7]. The performance of a thermoelectric device is controlled by the dimensionless thermoelectric figure of merit $ZT = \frac{S^2\sigma T}{\kappa}$ where S is the Seebeck coefficient, σ the electrical conductivity, T the temperature, and $\kappa = \kappa_e + \kappa_{ph}$ the total thermal conductivity which contains both electronic and phonon contributions. Thus a good thermoelectric material requires a large S , a high σ , and a low κ . In recent years, most efforts to improve ZT have focused on reducing the lattice thermal conductivity by enhancing the phonon scattering processes. This is achieved by different efficient modus operandi such as alloying [8,9], increasing the anharmonicity [10], or by introducing nano-inclusions/inhomogeneities into the matrix [11–13]. Since the first thermoelectric Bi₂Te₃ alloy has been discovered, the room-temperature ZT of bulk semiconductors has increased only marginally. However, recent studies in nanostructured thermoelectric materials have opened interesting pathways toward materials exhibiting large ZT [14–18]. The main ideas behind nanostructuring are twofold. First, it leads to quantum confinement of the carriers, inducing sharp peaks in the density of states, therefore giving rise to a simultaneous increase of both the S and σ . Second, the nanostructuring suppresses κ by increasing the phonon scattering. This strategy has, for instance, been applied to thin film superlattices such as Bi₂Te₃/Sb₂Te₃ [19,20], quantum dot superlattices PbSeTe/PbTe [21], and bulk alloys BiSbTe [22]. However, achieving quantum confinement in superlattices is not a simple and straightforward task [23]. As an example, it has been claimed in Ref. [24] that the strong enhancement

(with respect to the bulk compound) of both S and ZT in PbSeTe/PbTe quantum dot superlattices originated from the quantum confinement. It has been shown later [25], that the carrier densities were actually incorrect leading to a wrong interpretation of the measured Seebeck coefficients. Therefore it has been concluded that this PbSeTe/PbTe superlattice did not exhibit any confinement. Thus, experimental measurements that do not constitute a direct probe of the confinement effects should be analyzed carefully.

Recently, it has been argued that resulting from the two-dimensional carrier confinement in (SrTiO₃) _{x} /(SrTi_{0.8}Nb_{0.2}O₃) _{y} superlattices (x and y are, respectively, the number of undoped and Nb-doped layers), giant Seebeck coefficients have been measured [26,27]. In particular, in the extreme limit of a single Nb-doped layer ($y = 1$ and x varies), the measured S as a function of x could saturate at values almost six times larger than that of the bulk material. In addition, it has been concluded that the critical barrier thickness for quantum confinement was about 6.25 nm [16 unit cells of SrTiO₃ (STO)]. However, it is important to notice that the large increase of the Seebeck coefficient does not provide a direct signature of the two-dimensional (2D) quantum confinement. In this work, we demonstrate that the data could be explained assuming the absence (or weakness) of quantum confinement in these superlattices.

II. THEORETICAL MODELING OF THERMOELECTRIC PROPERTIES

In a recent study, we have shown that the thermoelectric properties of electron-doped STO (conductivity and Seebeck coefficient) could be well understood and reproduced within the framework of a realistic tight-binding (TB) Hamiltonian (three t_{2g} bands) that includes an electron-electron scattering mechanism and disorder treated in the Born approximation. The hopping integrals of the TB Hamiltonian were directly

*georges.bouzerar@univ-lyon1.fr

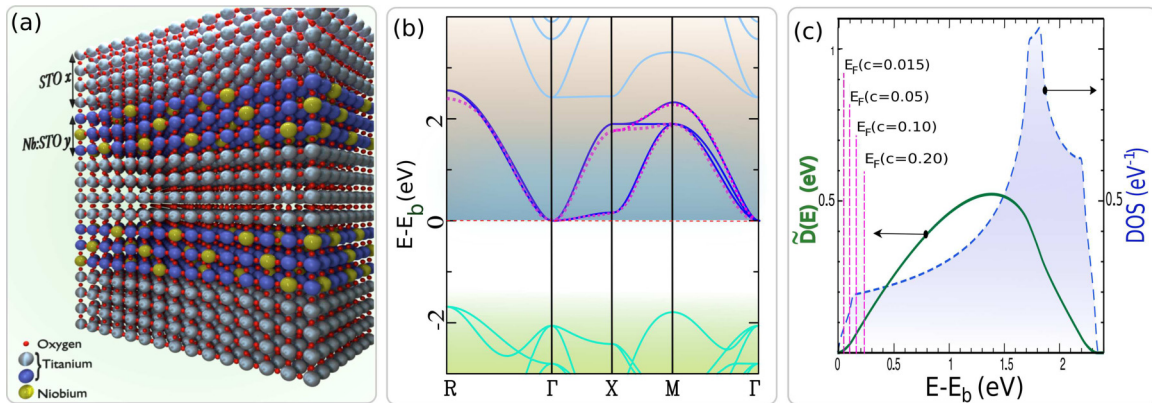


FIG. 1. (a) Schematic view of $(\text{STO})_x(\text{STO} : \text{Nb})_y$. (b) Bulk band structure from *ab initio* (continuous lines) and minimal tight binding (TB) model (pink dashed lines). Green lines correspond to the valence band and blue lines to the conduction bands. (c) TB calculations of the density of states and reduced Drude weight $\tilde{D}(E) = \frac{\hbar}{\sigma_0} D(E)$; E_b is the energy of the bottom of the conduction band. Vertical dashed lines indicate the position of the Fermi level for various carrier concentrations.

extracted from *ab initio* based studies [see Ref. [28] for details regarding the density functional theory (DFT) calculations]. The Hamiltonian reads $\hat{H}_0 = \sum_{\mathbf{k}, \alpha} \epsilon_{\alpha}^0(\mathbf{k}) c_{\mathbf{k}\alpha}^{\dagger} c_{\mathbf{k}\alpha}$ where α denotes the orbital index. The d_{xy} band dispersion is $\epsilon_{xy}^0(\mathbf{k}) = -2t_1[\cos(k_x a) + \cos(k_y a)] - 2t_2 \cos(k_z a) - 4t_3 \cos(k_x a) \cos(k_y a)$, where a is the lattice parameter. The two other bands (d_{yz} and d_{zx}) are obtained straightforwardly by a circular permutation of (x, y, z) . The hopping parameters obtained from Wannier projections are $t_1 = 0.277$ eV, $t_2 = 0.031$ eV, and $t_3 = 0.076$ eV. The formalism is further detailed in Refs. [28,29].

We now briefly summarize the procedure that allows one to calculate the Seebeck coefficient as a function of x , y , and temperature T . The calculations will be directly compared to the existing and available experimental data. The conductivity and the Seebeck coefficient are given by

$$\sigma(\mu, T) = - \int \Sigma(E, T) \frac{\partial f}{\partial E} dE, \quad (1)$$

$$S(\mu, T) = \frac{1}{eT\sigma(\mu, T)} \int \Sigma(E, T)(E - \mu) \frac{\partial f}{\partial E} dE, \quad (2)$$

where μ is the T -dependent chemical potential, f the Fermi-Dirac distribution, $\Sigma(E, T) = D(E)\tau(E, T)$ the transport distribution function, $D(E)$ the Drude weight (calculated at $T = 0$ K), and $\tau(E, T)$ the energy and temperature-dependent quasiparticle lifetime. We restrict ourselves to the weak disorder regime, a well justified approximation for samples exhibiting a good metallic behavior, it corresponds to $k_F l_e \gg 1$, where k_F is the Fermi wave vector and l_e the mean free path. In this regime, $D(E)$ can be well approximated by $D(E) \approx -\frac{\sigma_0}{N\hbar} \langle \hat{K}_x \rangle(E)$, where $\sigma_0 = \frac{e^2}{\hbar a} = 6258 \Omega^{-1} \text{cm}^{-1}$, N is the total number of sites, and $\hat{K}_x = -\frac{\partial^2 \hat{H}_0}{\partial \kappa_x^2}$ ($\kappa_x = k_x a$). It is worth mentioning that in the x direction, $D(E)$ is dominated by the d_{xy} and d_{xz} bands that contribute equally, while the d_{yz} band has a negligible contribution. The hopping integral in the x direction is indeed very small in the latter case. In Fig. 1 is plotted, (a) a schematic view of the superlattice structure, (b) the bulk band structure from *ab initio* (SIESTA) [30] and from the minimal TB model, and (c) the TB calculations for the bulk density of states and

reduced Drude weight. The position of the Fermi level for various carrier concentrations per unit cell is also shown.

The transport distribution function requires both the energy-dependent Drude weight and the electron lifetime $\tau(E, T)$. $\tau(E, T)$ has two contributions: $\frac{1}{\tau(E, T)} = \frac{1}{\tau_{\text{dis}}(E)} + \frac{1}{\tau_{\text{th}}(T, E)}$. $\tau_{\text{dis}}(E)$ denotes the effect of disorder resulting from the cationic substitutions and the presence of other defects (intrinsic, dislocations, grain boundaries) while $\tau_{\text{th}}(T, E)$ is the temperature-dependent part. Its origins are electron-electron (e-e) scattering and electron-phonon (e-ph) scattering. In oxides such as STO, several studies showing a T^2 -dependent resistivity suggest that the e-e mechanism prevails over the e-ph contribution up to relatively large temperatures [31–34]. This has been confirmed by the good agreement found between theory and experiment in Ref. [28]. From Fermi's golden rule we assume $\frac{\hbar}{\tau_{\text{dis}}(E)} = \frac{\pi W^2}{6} \rho(E)$ where $\rho(E)$ is the density of states and W the strength of the disorder. The T and E -dependent contribution is assumed to have the form $\frac{\hbar}{\tau_{\text{th}}(E)} = C \frac{(k_B T)^2}{E - E_b}$ where C is a dimensionless constant and E_b the energy at the bottom of the conduction band. For electron-doped STO it was shown that ($C = 24.5$, $W = 0.17$ eV) allows one to describe the physics quantitatively for a wide range of doping and dopants for both S and the σ . Note also that the strength of the disorder is small compared to the bandwidth which is of the order of 2.5 eV (see Fig. 1), thus it validates the weak disorder approximation. We now consider the scenario in which there is no 2D quantum confinement in $(\text{STO})_x(\text{STO} : \text{Nb})_y$. In order to calculate the S we assume a uniform carrier density per unit cell in the overall superlattice. Some indication that would support the absence of the confinement scenario is the experimental observations that suggest that Nb acts essentially as an electron reservoir in STO. This is supported by several DFT studies that show that the band structure, the density of states, and appear to be weakly affected by the substitution of Ti by Nb [38–40]. The Nb concentration per unit cell in the doped regions in the measured samples is $c_D = 0.20$ (Ref. [27]). Since we assume no 2D quantum confinement, the additional electrons introduced by the Nb atoms in the doped regions disperse in the entire compound, leading to a uniform carrier density per unit cell $c = \frac{y}{x+y} c_D$, which corresponds to the measured electron

density denoted n_{obs} in Table 1 of Ref. [27]. Note that our conclusions would not be changed significantly if the carrier concentration was not strictly uniform, but slightly modulated in the z direction. The important point is the absence of true quantum confinement, i.e., the electronic wave functions should not decrease exponentially in the undoped regions. It is important to stress that from now on, our theory is completely free of fitting parameters. We would like to emphasize that for the temperature range considered here (300–900 K), the Seebeck coefficient is almost independent from both C and W . Thus, the only relevant physical ingredients are (i) the details and accuracy of the band structure and (ii) the form of $\tau_{th}(T, E)$. If the electrons are really confined in the growth direction in these superlattices, we should expect a strong disagreement between our calculations and the experimental measurements, that would completely invalidate our procedure.

III. RULING OUT THE CONFINEMENT SCENARIO

In Fig. 2(a) the Seebeck coefficient at $T = 300$ K in the superlattice $(\text{STO})_x(\text{STO} : \text{Nb})_y$ is shown as a function of x for $y = 1, 2$, and 4. We clearly observe an overall good agreement between the measured values and the calculated ones. In Fig. 2(b) the data are now plotted as a function of $c = \frac{y}{x+y}c_D$; we find that the experimental data are well reproduced by the theoretical curve that assumes a uniform distribution of the carriers in the superlattice. The experimental data points exhibit some dispersion that may reflect the quality of the samples, the presence of native defects such as oxygen vacancies, dislocations, interface defects/deformations, sample history, and also the fact that the Nb concentration may fluctuate from sample to sample.

In Fig. 3 we now focus on the effect of the thickness of the Nb-doped region assuming a fixed value for the undoped one. We have now plotted the Seebeck coefficient as a function of y for two different temperatures, namely, $T = 300$ and 900 K; the number of undoped layers is set to $x = 17$. As we increase y the amplitude of the Seebeck coefficient decreases as a consequence of the increase of the overall carrier density. We again find a good agreement between the theory of a uniformly distributed electron gas and the experimental data; this agreement is even excellent at room temperature. In addition, we expect a saturation of the Seebeck coefficient for large y at $S_{\text{Bulk}}(c_D)$, which appears to be the case already for $y = 20$.

In the next figure, Fig. 4, we now focus on the particular case of a δ -doped compound, $y = 1$ for which a large increase of the Seebeck has been reported in Refs. [27,41]. We plot the enhancement factor $|\frac{S}{S_{\text{Bulk}}}|$ as a function of x and for two different temperatures ($T = 300$ and 900 K) where S_{Bulk} refers to the 20% doped bulk material that corresponds to $x = 0$. As mentioned above, the density of carriers cannot be precisely tuned experimentally, as a result of various mechanisms. Indeed, as seen from Hall measurements in Ref. [27], the density of electrons per doped layer can fluctuate by as much as 30% from sample to sample. Therefore, we include the effects of these variations by adding typically 1% additional carriers per unit cell. To be more specific, we perform the calculations for $c = \frac{y}{x+y}c_D + \delta c$ with δc up to 1% per unit cell. Note that performing realistic calculations including defects such as oxygen vacancies or dislocations would be extremely complicated and

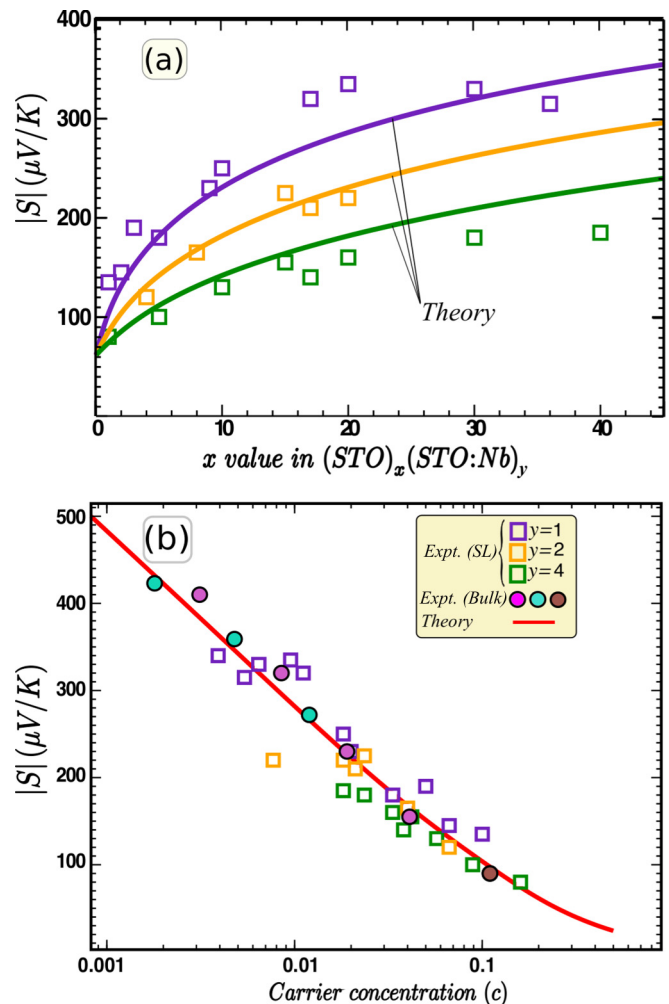


FIG. 2. (a) Seebeck coefficient at $T = 300$ K in $(\text{STO})_x(\text{STO} : \text{Nb})_y$ for $y = 1, 2$, and 4 and x varies from 0 to 50. Open squares are experimental data from Ref. [27]; the continuous lines are the TB calculations. (b) S as a function of $c = \frac{y}{x+y}c_D$, where $c_D = 0.20$ (Nb concentration in the doped regions). The experimental data are extracted from Refs. [35–37]. The continuous lines are the TB calculations.

demanding (requires extremely large supercells) and would go beyond the scope of the present paper. Let us now discuss the results. First notice that the experimental data, for a given value of x , are sample sensitive especially for large x (see full squares and empty squares); the enhancement factor can vary by about 20%. More generally, there is some dispersion in the experimental data, especially strong around $x = 10$. However, the agreement between theory and experiments is rather good, and even better at large temperature. As expected, the effect of additional carriers becomes more pronounced as we increase x . Thus, if δc is constant, it would result in the saturation of the enhancement factor at large x but it should be noticed that no critical or characteristic length scale can be extracted.

We now study the effect of temperature (it varies from $T = 300$ K to 900 K) on the Seebeck coefficient S in the superlattice $(\text{STO})_x(\text{STO} : \text{Nb})_1$, where x ranges from 0 (20% doped bulk material) to 36. The results are depicted in Fig. 5. First, regarding the bulk data ($x = 0$) we observe that the

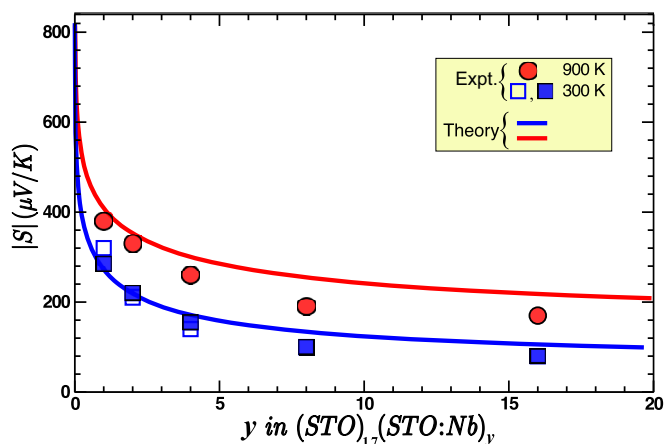


FIG. 3. Seebeck coefficient at $T = 300$ and 900 K in $(\text{STO})_{x=17}(\text{STO} : \text{Nb})_y$ as a function of y . Symbols are experimental data from Refs. [27,41] and continuous lines are the TB calculations.

theory agrees very well with the data from Ref. [42]. The measured bulk data of Ref. [41] are slightly smaller and appear to fluctuate with the temperature. Note that, for these data, the calculations would fit better assuming a slightly larger Nb concentration of the order of 23% instead of 20%. On the other hand, our calculated Seebeck coefficient agrees perfectly well with the experimental data for both $x = 1$ and $x = 3$, for the overall range of temperature. For $x = 9$ the calculated Seebeck coefficients are slightly larger (by 10%–15%). However, assuming a small additional amount of electrons ($\delta c = 1\%$ only), the agreement between theory and experiment now becomes excellent. Note also, that adding a small concentration of electrons for both $x = 1$ and $x = 3$ would only weakly affect the results (the average concentration would only weakly change). Regarding larger values of x ($x = 25, 30$, and 36) we first notice that the experimental data strongly fluctuates with the temperature, the average carrier concentrations in these superlattices are relatively low: 0.8%, 0.7%, and 0.5%, respectively. For $\delta c = 0$ the agreement is good

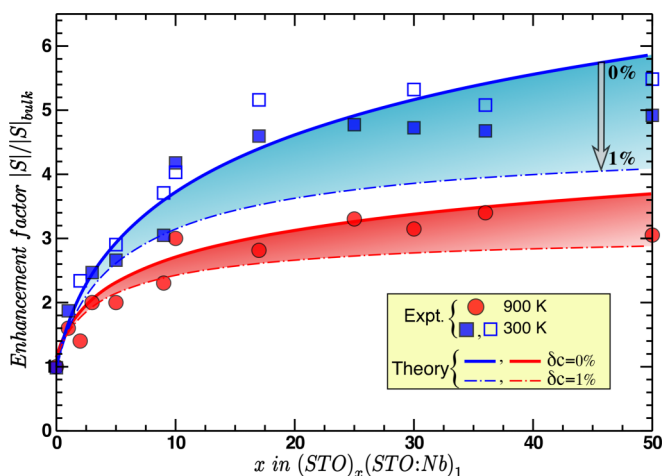


FIG. 4. Enhancement factor $|\frac{S}{S_{\text{Bulk}}}|$ of the Seebeck coefficient in $(\text{STO})_x(\text{STO} : \text{Nb})_1$ as a function of x for both $T = 300$ and 900 K. The filled region indicates the effects of an additional concentration of carriers δc up to 1%. The experimental data (symbols) are extracted from Refs. [27,41].

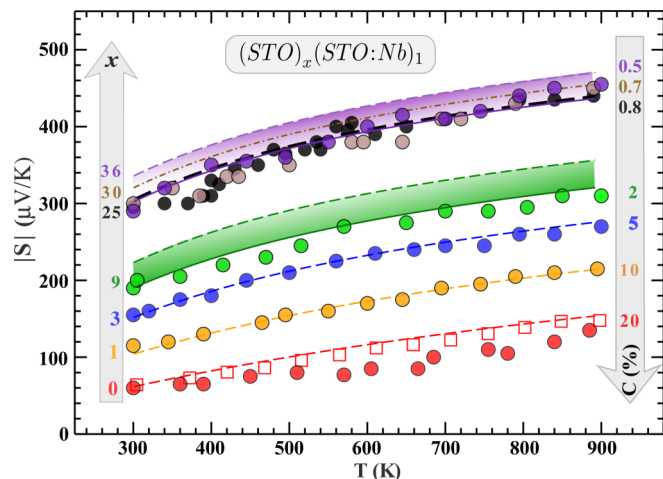


FIG. 5. Seebeck coefficient as a function of temperature in $(\text{STO})_x(\text{STO} : \text{Nb})_1$; x varies from 0 (20% doped bulk material) to 36. Filled and open symbols are experimental data from Refs. [41] and [42], respectively. Dashed and continuous lines are the TB calculations. The shaded regions correspond to the effect of δc up to 1% for $x = 9$ and δc up to 0.25% for $x = 36$. The effective concentration $c = \frac{y}{x+y}c_D$ is also plotted in the figure.

but the theoretical Seebeck coefficients are still slightly larger. However, by adding just 0.25% of carriers, the agreement between theory and experiment becomes excellent.

At this stage, we have shown that the experimental data can be well explained qualitatively and quantitatively assuming the absence of carrier confinement. To complete our demonstration, we now propose to analyze the effects of a full confinement of the electrons in the doped regions. This is achieved by assuming infinite potential barriers at the interfaces between doped and undoped regions. The calculated Seebeck coefficients (with and without confinement) and the experimental data are depicted in Fig. 6. Let us first compare

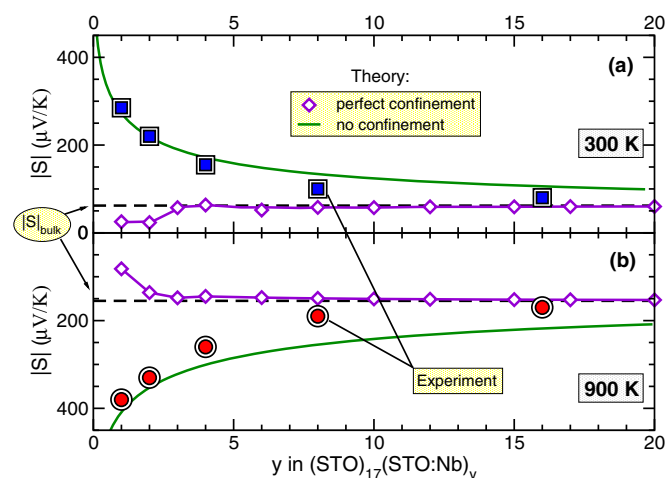


FIG. 6. Seebeck coefficient at (a) $T = 300$ K and (b) 900 K in $(\text{STO})_{x=17}(\text{STO} : \text{Nb})_y$ as a function of y . Filled symbols (squares and circles) are experimental data from Ref. [41]. The calculated Seebeck coefficients correspond to the green continuous lines (no confinement) and diamonds (perfect confinement of the carriers in the doped regions).

the two theoretical scenarios. Starting from large values of the doped region thickness y (bulk limit), clear opposite trends in the calculated Seebeck coefficients are visible as y is reduced toward δ doping. In the delocalized electron scenario, the Seebeck coefficient increases (in absolute value) as y is reduced. In contrast, in the fully confined electron picture, $|S|$ is almost flat down to $y = 5$ and then is strongly reduced to values much smaller than that of the bulk compound. As can clearly be seen, the apparent enhancement of the measured Seebeck coefficient is only consistent with the absence of the confinement scenario. In particular, for $y = 1$, the measured Seebeck coefficient was around $300 \mu\text{V/K}$ at 300 K and $400 \mu\text{V/K}$ at 900 K, while perfect confinement predicts only $25 \mu\text{V/K}$ at 300 K and $80 \mu\text{V/K}$ at 900 K. The suppression of the Seebeck coefficient for $y \leq 5$ in the confined scenario results from the fact that the two out-of-plane orbitals (d_{xz} and d_{yz}) are sent to higher energy. Mechanically, the carrier concentration in the lowest orbital increases, resulting in an upward shift of the Fermi energy and thus a reduction of the Seebeck coefficient.

IV. CONCLUDING REMARKS

To conclude, we have demonstrated that the recently reported giant increase of the Seebeck coefficients in (SrTiO₃)_x/(SrTi_{0.8}Nb_{0.2}O₃)_y superlattices is fully consistent only with the absence of 2D quantum confinement of the carriers in the doped regions. Indeed, in the electron confinement picture the opposite trend is found, namely, the suppression of the Seebeck coefficient. Our conclusion is further supported by the observation that the power factor (σS^2) measured in these superlattices is close to that of the bulk electron-doped STO [43]. It would be of great interest to confirm whether our scenario is correct by direct measurements such as transverse resistivity, angle-resolved photoemission spectroscopy, or by a direct probe of the depth profile of the carrier concentration. Oxide-based thermoelectric superlattices are promising materials for high- ZT devices but achieving a true 2D quantum confinement requires (i) a suitable choice of dopant that has a drastic effect on the host band structure in the vicinity of the Fermi level or (ii) a more appropriate choice for the undoped compound.

-
- [1] G. J. Snyder and E. S. Toberer, *Nat. Mater.* **7**, 105 (2008).
 [2] F. J. Di Salvo, *Science* **285**, 703 (1999).
 [3] M. S. Dresselhaus, G. Chen, M. Y. Tang, R. G. Yang, H. Lee, D. Z. Wang, Z. F. Ren, J.-P. Fleurial, and P. Gogna, *Adv. Mater.* **19**, 1043 (2007).
 [4] G. S. Nolas, J. Poon, and M. Kanatzidis, *Mater. Res. Soc. Bull.* **31**, 199 (2006).
 [5] H. J. Goldsmid, *Introduction to Thermoelectricity* (Springer, New York, 2010).
 [6] J. P. Heremans, B. Wiendlocha, and A. M. Chamoire, *Energy Environ. Sci.* **5**, 5510 (2012).
 [7] A. M. Dehkordi, *Mater. Sci. Eng., R* **97**, 1 (2015).
 [8] M. C. Steele and F. D. Rosi, *J. Appl. Phys.* **29**, 1517 (1958).
 [9] D. G. Cahill, F. Watanabe, A. Rockett, and C. B. Vining, *Phys. Rev. B* **71**, 235202 (2005).
 [10] J. Garg, N. Bonini, B. Kozinsky, and N. Marzari, *Phys. Rev. Lett.* **106**, 045901 (2011).
 [11] S. V. Faleev and F. Léonard, *Phys. Rev. B* **77**, 214304 (2008).
 [12] N. Wang, H. Chen, H. He, W. Norimatsu, M. Kusunoki, and K. Koumoto, *Sci. Rep.* **3**, 3449 (2013).
 [13] T. Zhang, Q. Zhang, J. Jiang, Z. Xiong, J. Chen, Y. Zhang, W. Li, and G. Xu, *Appl. Phys. Lett.* **98**, 022104 (2011).
 [14] L. D. Hicks and M. S. Dresselhaus, *Phys. Rev. B* **47**, 16631 (1993).
 [15] G. D. Mahan and J. O. Sofo, *Proc. Natl. Acad. Sci. USA* **93**, 7436 (1996).
 [16] N. Mingo, *Appl. Phys. Lett.* **84**, 2652 (2004).
 [17] S. Farhangfar, *J. Phys. D: Appl. Phys.* **44**, 125403 (2011).
 [18] J. Zhou, R. G. Yang, G. Chen, and M. S. Dresselhaus, *Phys. Rev. Lett.* **107**, 226601 (2011).
 [19] R. Venkatasubramanian, *Phys. Rev. B* **61**, 3091 (2000).
 [20] R. Venkatasubramanian, E. Siivola, and T. Colpitts, *Nature (London)* **413**, 597 (2001).
 [21] T. C. Harman, P. J. Taylor, M. P. Walsh, and B. E. LaForge, *Science* **297**, 2229 (2002).
 [22] B. Poudel *et al.*, *Science* **320**, 634 (2008).
 [23] C. J. Vineis, A. Shakouri, A. Majumdar, and M. G. Kanatzidis, *Adv. Mater.* **22**, 3970 (2010).
 [24] T. C. Harman, P. J. Taylor, D. L. Spears, and M. P. Walsh, *J. Electron. Mater.* **29**, L1 (2000).
 [25] C. J. Vineis, T. C. Harman, S. D. Calawa, M. P. Walsh, R. E. Reeder, R. Singh, and A. Shakouri, *Phys. Rev. B* **77**, 235202 (2008).
 [26] H. Ohta *et al.*, *Nat. Mater.* **6**, 129 (2007).
 [27] Y. Mune, H. Ohta, K. Koumoto, T. Mizoguchi, and Y. Ikuhara, *Appl. Phys. Lett.* **91**, 192105 (2007).
 [28] G. Bouzerar, S. Thébaut, Ch. Adessi, R. Debord, M. Apreutesei, R. Bachelet, and S. Pailhès, *Euro. Phys. Lett.* **118**, 67004 (2017).
 [29] Z. Zhong, A. Tóth, and K. Held, *Phys. Rev. B* **87**, 161102(R) (2013).
 [30] J. M. Soler, E. Artacho, J. D. Gale, A. García, J. Junquera, P. Ordejón, and D. Sánchez-Portal, *J. Phys.: Condens. Matter* **14**, 2745 (2002).
 [31] A. Baratoff and G. Binnig, *Physica B (Amsterdam)* **108**, 1335 (1981).
 [32] D. van der Marel, J. L. M. van Mechelen, and I. I. Mazin, *Phys. Rev. B* **84**, 205111 (2011).
 [33] E. Mikheev, B. Himmetoglu, A. P. Kajdos, P. Moetakef, T. A. Cain, C. G. Van de Walle, and S. Stemmer, *Appl. Phys. Lett.* **106**, 062102 (2015).
 [34] S. N. Klimin, J. Tempere, D. van der Marel, and J. T. Devreese, *Phys. Rev. B* **86**, 045113 (2012).
 [35] T. A. Cain, A. P. Kajdos, and S. Stemmer, *Appl. Phys. Lett.* **102**, 182101 (2013).
 [36] S. Ohta, T. Nomura, H. Ohta, and K. Koumoto, *J. Appl. Phys.* **97**, 034106 (2005); *Appl. Phys. Lett.* **87**, 092108 (2005).
 [37] B. Jalan and S. Stemmer, *Appl. Phys. Lett.* **97**, 042106 (2010).
 [38] D. I. Bilc, C. G. Floare, L. P. Zárbo, S. Garabagiu, S. Lemal, and P. Ghosez, *J. Phys. Chem. C* **120**, 25678 (2016).

- [39] A. Kinaci, C. Sevik, and T. Çağın, *Phys. Rev. B* **82**, 155114 (2010).
- [40] K. Ozdogan, M. Upadhyay Kahaly, S. R. Sarath Kumar, H. N. Alshareef, and U. Schwingenschlögl, *J. Appl. Phys.* **111**, 054313 (2012).
- [41] H. Ohta, *Phys. Status Solidi B* **245**, 2363 (2008).
- [42] M. Sonne, N. Van Nong, Z. He, N. Pryds, and S. Linderoth, Improvement of Niobium Doped SrTiO₃ by Nanostructuring, in *Proceedings of 8th European Conference on Thermoelectrics, Como, Italy* (2010), pp. 175–178.
- [43] W. S. Choi, H. Ohta, and H. N. Lee, *Adv. Mater.* **26**, 6701 (2014).